# Three-dimensional imaging of atoms using source waves from deeply buried atoms and overcoming multiple-scattering effects

H. Huang, Hua Li, and S. Y. Tong
*Department of Physics and Laboratory for Surface Studies, University of Wisconsin–Milwaukee, Milwaukee, Wisconsin 53201*
(Received 22 February 1991)

A method for image reconstruction is applied to the Cu(111) system. We show that effects of multiple scattering and diffraction of source waves emitted from deeply buried atoms produce strong artifacts making single-energy image reconstruction unreliable. Using the small-window energy-extension process, we overcome the above difficulties and obtain single-atom images with less than 1-Å spatial resolution.

Recent works have demonstrated that three-dimensional (3D) atomic images can be constructed by inverting diffraction patterns of electrons emitted from localized sources embedded in a material.[1–9] However, multiple scattering and interference from nearby atoms cause shifts in the image position and produce artifacts which hamper image identification in unknown systems.[1,5,7] In the forward-scattering geometry, the problem of interference from nearby atoms is particularly severe for source atoms located a few atomic layers ($N \geq 3$ monolayers) below the surface because, at high energies, the scattering is predominantly confined to a narrow cone in the forward direction and the number of scatterers in this cone increases rapidly as the depth of the source atoms increases. With many nearby atoms, images are formed at $\pm\mathbf{r}_i$ as well as $\pm(\mathbf{r}_i-\mathbf{r}_j)$ where $\mathbf{r}_i$ or $\mathbf{r}_j$ is measured from the source atom to the $i$ or $j$ scatterer, respectively. Since there are many possible combinations of $\pm(\mathbf{r}_i-\mathbf{r}_j)$, these mixed-index images can obscure the proper image at a particular $\mathbf{r}_i$.

There is also interest in image reconstruction using electrons emitted from atoms in a slab or thin film.[1,4–7] The problem is compounded because in a slab or thin film the surface breaks the symmetry in the normal direction causing the environment of atoms in each layer to be different. The source waves from inequivalent atoms produce different interference patterns that must be processed separately and then incoherently added to form a single image. This generally degrades the quality of the atomic image.

This paper illustrates the problems of interference from nearby atoms; buried source atoms and multiple scattering are overcome in the forward-scattering geometry by an image processing scheme introduced recently.[1,9] This scheme, called small-window energy-extension process (SWEEP), was first used to improve image resolution and reduce noise.[1,9] The method has been demonstrated to work successfully for the Si(111)-$(\sqrt{3}\times\sqrt{3})R30°$-$B$ system: A system in which single-scattering events dominate because the $B$ atoms occupy the second atomic layer.[1,9] Furthermore, since there is only one $B$ layer, all sources waves are equivalent.[8,9] Here, we demonstrate the SWEEP method in a system having all the problems listed above. The example chosen for this demonstration is a Cu(111) slab.

The starting point of this technique is the acquisition of angular $(\theta,\phi)$ scans of electron-diffraction data at constant emission energy from a localized source (i.e., atom) embedded in a material. For the purpose of image reconstruction, the preferred mode of collecting x-ray photoemission spectroscopy (XPS) diffraction data is to rotate the crystal while keeping the directions of photon incidence and electron exit fixed. This collection mode eliminates the anisotropy in the outgoing unscattered wave from an initial core level (i.e., the excitation matrix element effect is eliminated). In a rotate-crystal angular scan, the source wave is continuously changing, consequently the diffraction pattern is not a single hologram. We will not use the Helmholtz-Kirchoff integral for holographic reconstruction used by other workers,[2–4,6] instead we will apply a 3D Fourier transformation (FT) to the diffraction pattern:[1,9]

$$\phi(\mathbf{R})=\left|\int \chi(\mathbf{k})\delta(k-k_0)e^{i\mathbf{k}\cdot\mathbf{R}}d^3k\right|, \tag{1}$$

where $\chi(\mathbf{k})\delta(k-k_0)=[I(k_0)/\cos\theta-A]/A$. Here, $I(k_0)$ is a measured or calculated XPS intensity at $k=k_0$, the $[\cos\theta]^{-1}$ factor is to account for the geometric condition of measurement, $A$ is the angle-averaged value of $I(k_0)/\cos\theta$, and $k_0=[(2m/\hbar^2)E]^{1/2}$ is the photoelectron's wave vector. Integrating out the $\delta$ function and setting $k_0^2 d\Omega = d\mathbf{k}_\parallel/\cos\theta$, we obtain

$$\phi(\mathbf{R})=\left|\int \frac{\chi(k_0\hat{\mathbf{k}})e^{ik_0\hat{\mathbf{k}}\cdot\mathbf{R}}}{\cos\theta}dk_x dk_y\right|. \tag{2}$$

Due to the highly peaked nature of the forward-scattering factor, the interference fringes in a small angular cone $\Omega_c$ surrounding each focusing peak are dominated by the diffraction from an atom or atoms lying along that particular emitter-scatterer direction.[10–16] Widening the angular cone simply adds interference fringes from atoms along other focusing directions thereby increasing the noise in the image reconstruction. For a given usable

 

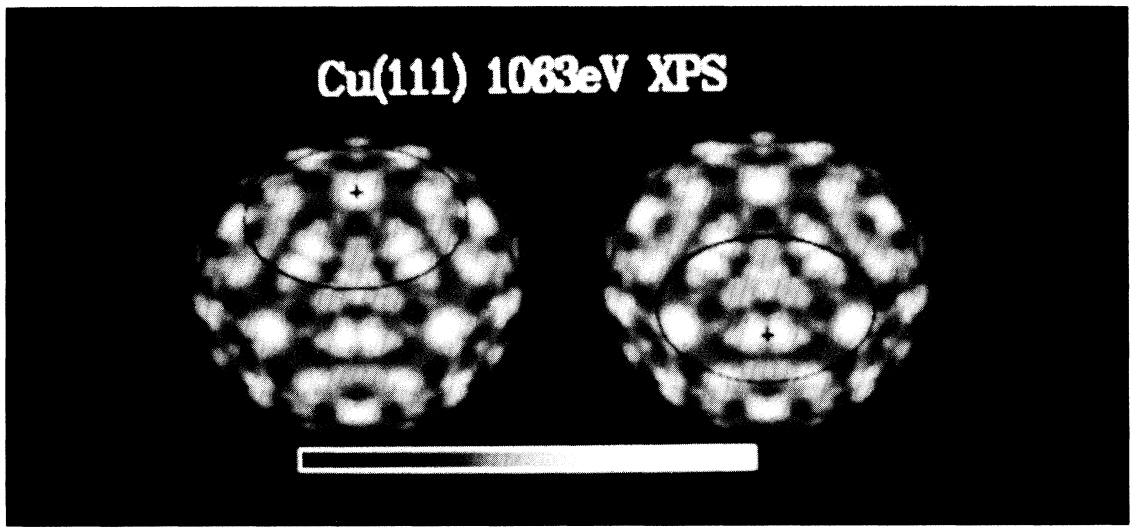


FIG. 1. Angular $(\theta,\phi)$ plot of a 20-layer Cu(111) slab, crosses mark 35.3° (left) and 19.5° (right) focusing directions, projected circles have $\theta_c=40°$.

$\Omega_c$, the limit of spatial resolution is given by $\Gamma_\perp=\pi/(k_0\sin\theta_c)$ and $\Gamma_\parallel=2\pi/[k_0(1-\cos\theta_c)]$, where $\Gamma_\perp$ and $\Gamma_\parallel$ refer to the full width at half magnitude (FWHM) of the image perpendicular and parallel to the emitter-scatterer directions, respectively.[1,9] For a 1000-eV photoelectron with a **k**-space angular cone of $\theta_c=40°$, $\phi_c=0,2\pi$, the above equations give $\Gamma_\perp=0.30$ Å and $\Gamma_\parallel=1.66$ Å. The images are thus elongated towards the origin (i.e., emitter) with the resolution along the emitter-scatterer direction particularly poor. Note that $\theta_c$ is half the polar angle of the solid cone (see Ref. 1, Fig. 6).

In the SWEEP method, interference fringes in $\Omega_c$ at different energies are joined together to form atomic images. Figure 1 shows diffraction data and angular cones of $\theta_c=40°$, $\phi_c=0,2\pi$ surrounding the 35.3° (left) and 19.5° (right) focusing directions of Cu(111). The diffraction patterns are calculated for emission from the Cu(2$p$) core level. The photon incident direction and the electron exit angle are fixed at 70° apart while the crystal is rotated to generate the $2\pi$ hemispherical scan. The photon is $p$ polarized. The calculations are based on the multiple-scattering slab method, which includes all orders of forward and back-scattering events in a 20-layer Cu(111) slab.[17,18] Excitation selection $p\rightarrow d$ and $p\rightarrow s$ matrix elements are explicitly evaluated. The atomic arrangements along main crystallographical directions of the Cu(111) slab are shown schematically in Fig. 2.[19] The image of the $\alpha$th atom from joining together multienergy intervals is given by[1,9]

$$\phi^{\alpha}_{R_\alpha}(\mathbf{R})=\mathcal{D}\left|\sum_{n=1}^{N}\int_{\Omega_c}\frac{\bar{G}_\alpha(k_n\hat{\mathbf{k}})e^{-ik_nR_\alpha}e^{ik_n\hat{\mathbf{k}}\cdot\mathbf{R}}}{\cos\theta}dk_{n,x}dk_{n,y}\right|, \tag{3}$$

where $k_n=[(2m/\hbar^2)E_n]^{1/2}$ and the integral is over the solid angle $\Omega_c$. The quantity $\mathcal{D}$ is the density of the energy points, given by $\mathcal{D}=(k_N-k_1)/(N-1)$, where $N$ is the number of energy points. The function $\bar{G}_\alpha(k_n\hat{\mathbf{k}})=[G_\alpha(k_n\hat{\mathbf{k}})-A']/A'$, where $A'$ is the average value of $G_\alpha(k_n\hat{\mathbf{k}})$ inside the angular cone and $G_\alpha(k_n\hat{\mathbf{k}})$ is the phase-shift corrected function given by

$$G_\alpha(k_n\hat{\mathbf{k}})=\chi(k_n\hat{\mathbf{k}})/p_\alpha(k_n\hat{\mathbf{k}}) . \tag{4}$$

In Eq. (4), $p_\alpha(k_n\hat{\mathbf{k}})$ is the phase shift correction function defined earlier.[1,8] Note that the central axis of $\Omega_c$ is along the focusing direction of the $\alpha$th atom. From Eq. (7) of Ref. 7, it is clear that the phase factor $e^{-ik_nR_\alpha}$ introduced in Eq. (3) exactly cancels the energy-dependence phase in $G_\alpha(k_n\hat{\mathbf{k}})$. This means that what remains in the integrand is a pure plane-wave front that is joined together and extended by Eq. (3). It is then easy to see that a Fourier transformation of this extended plane-wave front will give a better resolution.

In Eq. (3), the function $\Phi^{\alpha}_{R_\alpha}(\mathbf{R})$ requires the magnitude $|\mathbf{R}_\alpha|$ as an input. We can find $R_\alpha$ by using trial values $R_i$. We start with selecting energies $E_1,E_2,\ldots,E_N$ whose wave vectors $k_1,k_2,\ldots k_N$ are evenly spaced: i.e., $k_2-k_1=k_3-k_2=\cdots=\mathcal{D}$. (Here, $E_1$ is the smallest energy.) Furthermore, we require that no gap exists in $\Delta k$

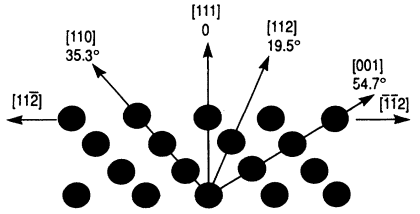


FIG. 2. Schematic Cu(111) side view showing focusing directions.

along the focusing direction $\alpha$ which means $E_{i+1} \leq E_i/\cos^2\theta_c$.[1,9] It is, of course, acceptable to have overlapping $\Delta k$ in the choice of $E_i$.[9] Using Eq. (3), with $R_i$ substituting for $R_\alpha$, we note that $\Phi^\alpha_{R_i}(\mathbf{R})$ is a periodic function:

$$\Phi^\alpha_{R_i+L}(\mathbf{R}) = \Phi^\alpha_{R_i}(\mathbf{R}) \tag{5}$$

with $L = 2\pi/\mathcal{D}$. As an example, for Cu(111), we choose 14 energies, with $E_1 = 263$ eV, $E_2 = 334$ eV, ..., $E_{14} = 1836$ eV, and $\mathcal{D} = 1.05$ Å$^{-1}$, giving a period of $L = 5.96$ Å. This means the trial values of $R_i$ need only to cover this range $L$.

The choice of a uniform $\Delta k$ is not an enabling requirement. An advantage of the choice is that with it, the trial values $R_i$ could be in a completely arbitrary range. For example, if the correct bond distance is $R_\alpha = 2.55$ Å, and the period is $L = 6$ Å, one could choose $R_i$ from 5 to 11 Å and still find the correct $R_\alpha$. We illustrate this point in the following example. A plot of $\Phi^\alpha_{R_i}(R)$ is shown in Fig. 3 for the 20-layer Cu(111) slab with the origin at the source atom and *with* $\mathbf{R}$ *measured along the* 35.3° *focusing direction.* An angular cone of $\theta_c = 40°$ and $\phi_c = 0, 2\pi$ is used. The periodic nature of the function $\Phi^\alpha_{R_i}(R)$ is clearly evident in the figure. The contours are drawn in an arbitrary scale with a maximum of 100 and decrease in steps of 5% (dark spot), 10%, 30%, and 50% from the maximum value. Since we expect that at the trial value of $R_i = R_\alpha$ the function $\Phi^\alpha_{R_i}(\mathbf{R})$ will peak at $\mathbf{R} = \mathbf{R}_\alpha$, we look for the maximum of this function along the dashed line $R_i = |\mathbf{R}|$ or the equivalent lines $R_i \pm nL = |\mathbf{R}|$, $n = 0, 1, 2 \ldots$. The intensity of $\Phi^\alpha_{R_i}(\mathbf{R})$ along a dashed line is shown in Fig. 4. The maximum value is at $|\mathbf{R}| = 2.50$ Å which is the determined $|\mathbf{R}_\alpha|$, compared to the correct nearest-neighbor distance of 2.55 Å. The error bar (shaded area) of $|\mathbf{R}_\alpha|$ is ±0.3 Å. Noise due to multiple scattering or nearby scatterers contributes to other high intensity regions in the 2D contour plot. However, only maxima along the dashed lines $R_i \pm nL$ need to be considered.

The shape of the curve in Fig. 4 depends on the energy range $E_N - E_1$ and not the number of energies used in the SWEEP process. The larger the energy range, the sharper the peak near 2.55 Å and the higher the peak intensity. The (smaller) peak at 1.0 Å is noise; its intensity will decrease as the energy range increases.

A different energy-extension scheme in which an integral over $k$ is performed has been proposed for the back-scattering[20,21] and forward-scattering geometries.[22] This is equivalent to *forming the atomic images directly along the* $R_i = |\mathbf{R}|$ *line.* From the contour plot in Eq. (3), we note that in the forward-scattering geometry, the intensity contours form a ridge in this direction, thus making it the least attractive direction for image formation because $\Phi^\alpha_{R_i}(\mathbf{R})$ is particularly slow varying along this line.

We first show the images reconstructed from single energies: Fig. 5 shows image intensity curves along the 35.3° focusing direction. The emitter is at the origin and the correct nearest-neighbor distance is 2.55 Å away (marked by an arrow). In the figure the reconstruction from a 20-layer slab, source atoms located in the second, third, and fourth layers are shown, respectively, from left to right. The upper and lower panels correspond to 500 and 1501 eV, respectively. The angular window used is again $\theta_c = 40°$, $\phi_c = 0, 2\pi$.

We notice substantial errors in the image positions that are formed: e.g., (i) no clear image is formed at 2.55 Å (fourth-layer source at 500 eV); (ii) the highest peak does not correspond to the correct distance (slab, third- and

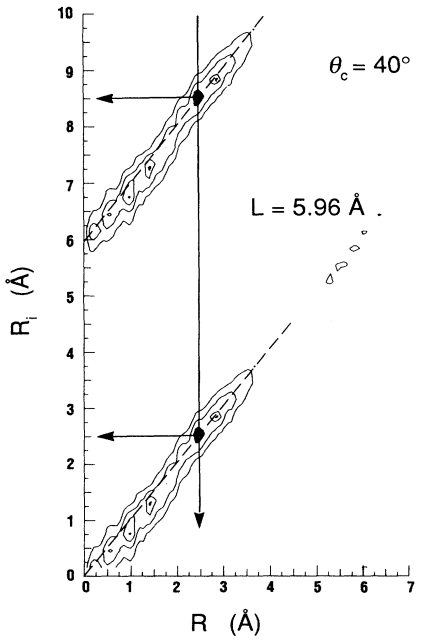


FIG. 3. Contours of $\Phi^\alpha_{R_i}(\mathbf{R})$ for a Cu(111) slab with $\hat{\mathbf{R}}$ along the 35.3° focusing direction. The dark spots mark the maxima along $R_i \pm nL = |\mathbf{R}|$ lines.

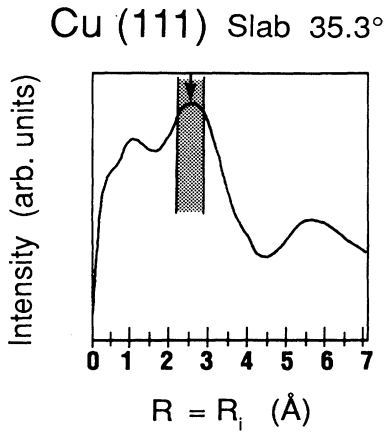


FIG. 4. Intensity scan along a $R_i \pm nL = |\mathbf{R}|$ line; arrow points to its maximum value, $\theta_c = 40°$.

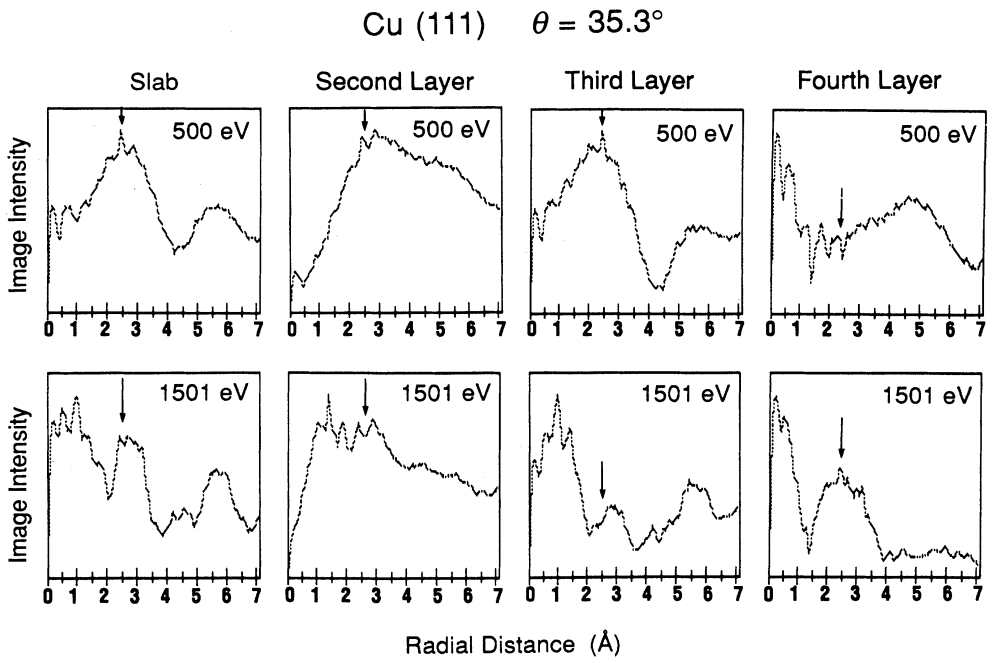


FIG. 5. Radial intensity plots along 35.3° focusing direction, emitter at origin, nearest-neighbor scatterer position marked by an arrow. A small window $\theta_c = 40°$ is used.

fourth-layer sources at 1501 eV); and (iii) the arrows point to dips in compound features. It is clear that the combination of multiple scattering and scattering from nearby atoms produce a high level of noise which disables image reconstruction using data at a single energy. When an image peak is not dominant in the intensity versus radial distance plot, it creates ambiguity in the structural determination of unknown systems.

To demonstrate the ability of the SWEEP method to overcome these difficulties, we use 14 energies, from 263 to 1836 eV, with $\mathcal{D}=1.05$ Å$^{-1}$. We use the contour map of $\Phi^{\alpha}_{R_i}(R)$ (e.g., see Figs. 3 and 4) to determine $R_\alpha$. With $R_\alpha = 2.50$ Å, we form the image $\Phi^{\alpha}_{R_\alpha}(\mathbf{R})$ according to Eq. (3). Figure 6 shows the radial-image function of $\Phi^{\alpha}_{R_\alpha}(\mathbf{R})$ along $\theta = 35.3°$: the improvement in the image quality and resolution is dramatic; noise is largely eliminated and a dominant peak is formed with a FWHM ranging from 0.68 to 0.90 Å. In the process of "washing" out artifacts, it is best to try different energy ranges and energy points. As these increase, one should find the "image" peak increases in intensity and those of artifacts decrease. In addition, the value of $R_\alpha$ can be more accurately determined with a wider energy range. Radial intensity plots along the 19.5° focusing direction for single energies and 14 energies SWEEP results are reported elsewhere.[1]

The atomic images along a cut plane normal to the surface and passing through the atoms are presented in Fig. 7 where the emitter (cross) and nearest-neighbor atom (circle) along the 35.3° direction are shown (left panel) for

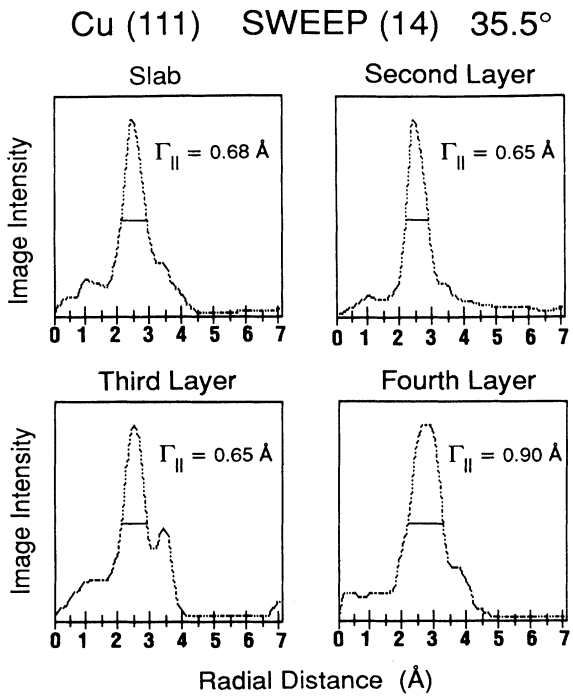


FIG. 6. Radial intensity plot along 35.3° for a 20-layer Cu(111) slab from 14 energies SWEEP for source atoms in all layers (slab), in second, third, and fourth layers, respectively. The emitter is at the origin.

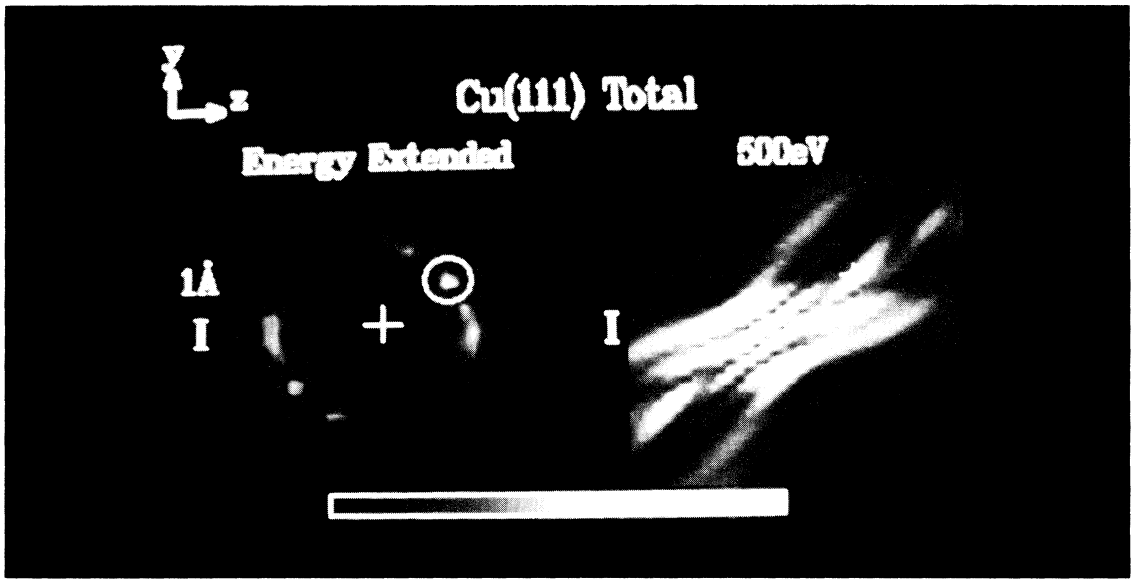


FIG. 7. Left: Nearest-neighbor atomic image (spot inside circle) along 35.3° direction from 14 energies SWEEP in $YZ$ plane. Distance between cross (emitter) and center of circle is the correct bond length 2.55 Å. Right: Single-energy atomic image, crosses mark emitter and correct scatterer positions. Sources in all layers of slab.

a Cu(111) slab. The only physical region is along the 35.3° direction; the artifacts at other polar angles and those on the twin image side can be discarded. The diameter of the circle is 1.2 Å. By comparison, the poorly resolved single-energy image is shown in the right panel (its radial-intensity plot along 35.3° is the one shown in Fig. 5, upper left). The reduction of noise along the physical direction (i.e., 35.3°) as well as a marked improvement in the resolution are evident.

A similar comparison is shown in Fig. 8 for the nearest-neighbor atom along the 19.5° direction. For the image shown, the source atom is located in the third atomic layer. Again, the diameter of the circle is 1.2 Å. The single-energy atomic image is shown in the right panel. The radial intensity plot of this image can be found in Ref. 1. Note that in Figs. 7 and 8 the surface normal (i.e., $\hat{\mathbf{Z}}$) points towards the right.

In the SWEEP method, we decouple the determination of $R_\alpha$ from the image resolution. The process is to first find $R_\alpha$ from the contour plots in Fig. 3. For a given

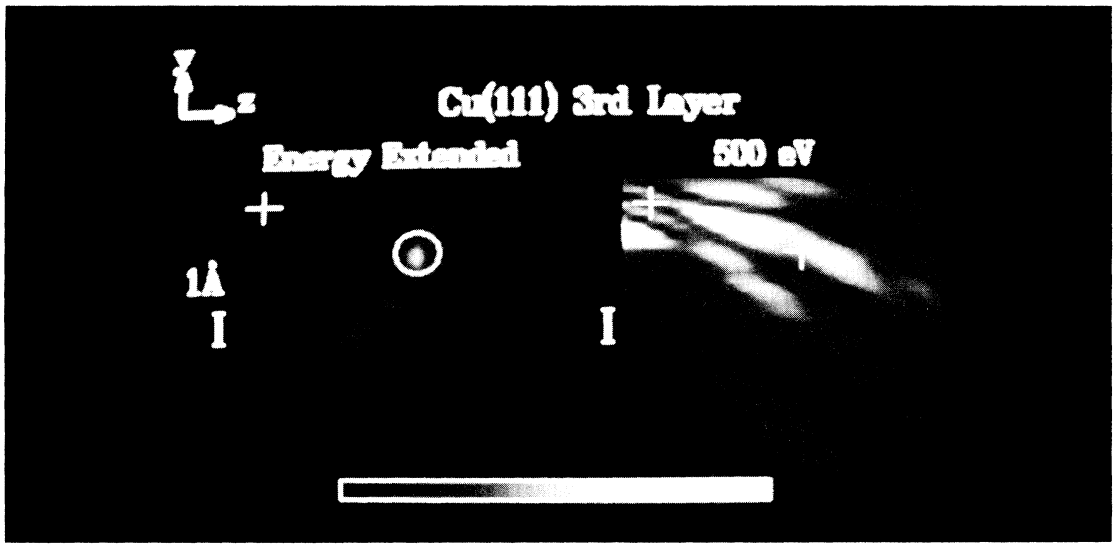


FIG. 8. Same as in Fig. 7 except along the 19.5° direction. Source atoms located in third layer only. The distance between emitter and scatterer is 4.42 Å.

value of $R_\alpha$, Eq. (3) produces atomic images with a high resolution. We have demonstrated that for a Cu(111) slab, noise from the reconstruction process is a major difficulty and that images processed from single-energy interference data contain strong artifacts that make structural determination questionable. By contrast, using the SWEEP method on this system produces resolution of better than 1 Å and $R_\alpha$ is determined to within $\pm 0.3$ Å. The latter is only moderately impressive when compared to results of diffraction techniques (e.g., LEED, x-ray scattering, photoelectron diffraction, etc.) where bond distances are determined to a precision of 0.05–0.1 Å. However, imaging is a direct structural tool, thus avoiding the trial-and-error process necessary in diffraction techniques. The priority in imaging is not high-precision bond-distance determination (this can be done better by diffraction methods). Rather, the primary goal is to achieve very high-resolution images so individual atoms appear separately thus allowing the geometric configuration to be clearly viewed. Once the structural configuration is revealed, bond distances can be fine tuned by diffraction methods.

The SWEEP method also brings out the unique features of a "lensless" microscope: By using a small $\Omega_c$ around a focusing direction and extending the energies (i.e., $\Delta\mathbf{k}$), we are able to join together interference fringes exclusive to the chain of atoms along a specific direction. Therefore, noise is kept low while the resolution is improved as $\Delta\mathbf{k}$ increases. Since lenses are not used, aberration is not an issue. In principle, the SWEEP method can reach any desirable resolution in the emitter-scatterer direction,[1,9] provided data at extended-energy ranges are available.

This work was supported in part by the Office of Naval Research Grant No. N00014-90-J-1749.

[1]See, for example, S. Y. Tong, H. Huang, and Hua Li, in *Advances in Surface and Thin Film Diffraction,* edited by T. C. Huang, P. I. Cohen, and D. J. Eaglesham, MRS Symposia Proceedings No. 208 (Materials Research Society Series, Pittsburgh, 1991).

[2]J. J. Barton, Phys. Rev. Lett. **61**, 1345 (1988).

[3]D. K. Saldin and P. L. de Andres, Phys. Rev. Lett. **64**, 1270 (1990).

[4]G. R. Harp, D. K. Saldin, and B. P. Tonner, Phys. Rev. Lett. **65**, 1012 (1990).

[5]C. M. Wei, T. C. Zhao, and S. Y. Tong, Phys. Rev. Lett. **65**, 2278 (1990).

[6]G. R. Harp, D. K. Saldin, and B. P. Tonner, Phys. Rev. B **42**, 9199 (1990).

[7]C. M. Wei, T. C. Zhao, and S. Y. Tong, Phys. Rev. B **43**, 6354 (1991).

[8]S. Y. Tong, C. M. Wei, T. C. Zhao, H. Huang, and Hua Li, Phys. Rev. Lett. **66**, 60 (1991).

[9]S. Y. Tong, Hua Li, and H. Huang (unpublished).

[10]W. F. Egelhoff, Jr., Phys. Rev. Lett. **59**, 559 (1987).

[11]H. C. Poon and S. Y. Tong, Phys. Rev. B **30**, 6211 (1984).

[12]S. Y. Tong, H. C. Poon, and D. R. Snider, Phys. Rev. B **32**, 2096 (1985).

[13]M. L. Xu and M. A. Van Hove, Surf. Sci. **207**, 215 (1989).

[14]S. A. Chambers, in *Advances in Physics,* edited by S. Doniach (Taylor and Francis, London, 1991).

[15]C. S. Fadley, in *Synchrotron Radiation Research: Advances in Surface Science,* edited by R. Z. Bachrach (Plenum, New York, 1990).

[16]S. Y. Tong, M. W. Puga, H. C. Poon, and M. L. Xu, in *Chemistry and Physics of Solid Surfaces VI,* edited by R. Vanselow and R. Howe (Springer, New York, 1986).

[17]S. Y. Tong, C. H. Li, and A. R. Lubinsky, Phys. Rev. Lett. **39**, 498 (1977).

[18]C. H. Li, A. R. Lubinsky, and S. Y. Tong, Phys. Rev. B **17**, 3128 (1978).

[19]X. D. Wang, Z. L. Han, B. P. Tonner, Y. Chen, and S. Y. Tong, Science **248**, 1129 (1990).

[20]J. J. Barton and L. J. Terminello, in *The Structure of Surfaces III,* edited by S. Y. Tong, M. A. Van Hove, X. Xie, and K. Takayanagi (Springer, Berlin, 1991).

[21]J. J. Barton, J. Electron Spectrosc. Relat. Phenom. **51**, 37 (1990).

[22]S. Hardcastle, Z. L. Han, G. R. Harp, J. Zhang, B. L. Chen, D. K. Saldin, and B. P. Tonner, Surf. Sci. Lett. **245**, L190 (1991).

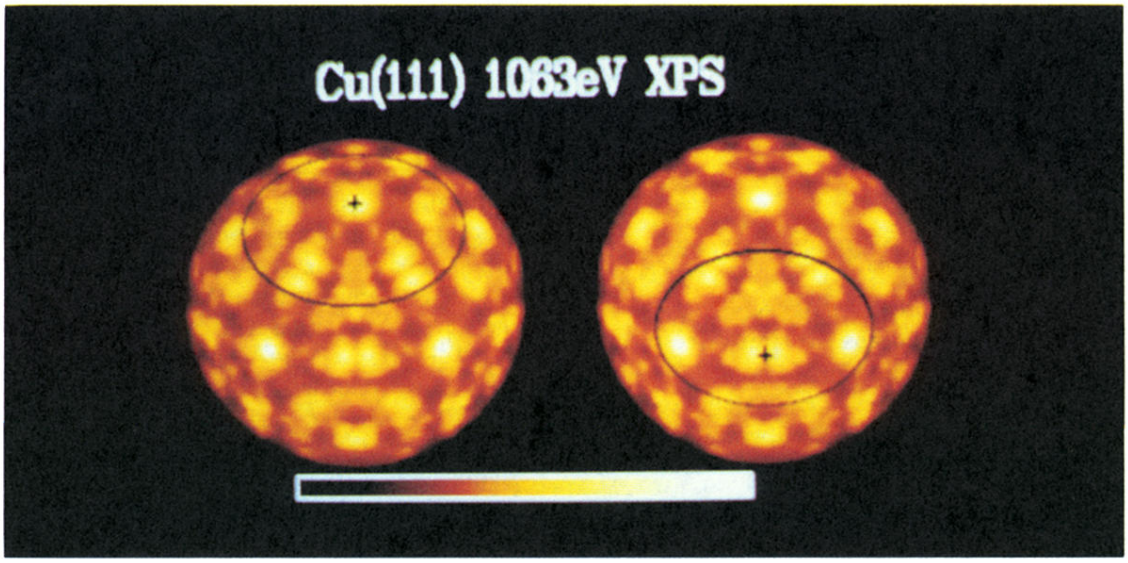


FIG. 1. Angular $(\theta,\phi)$ plot of a 20-layer Cu(111) slab, crosses mark 35.3° (left) and 19.5° (right) focusing directions, projected circles have $\theta_c = 40°$.

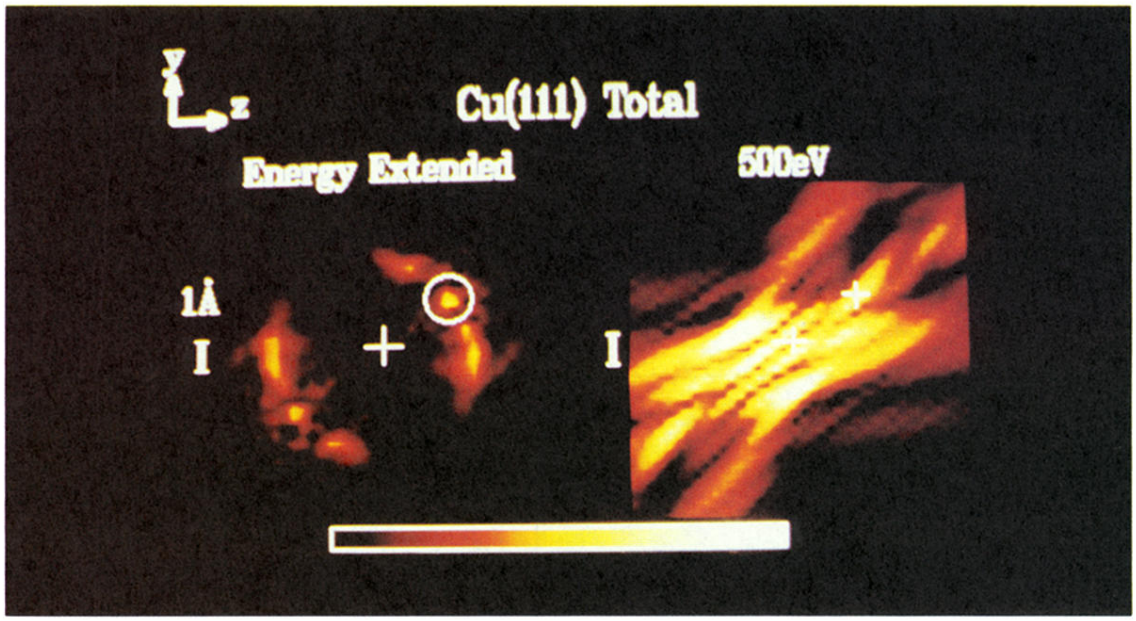


FIG. 7. Left: Nearest-neighbor atomic image (spot inside circle) along 35.3° direction from 14 energies SWEEP in *YZ* plane. Distance between cross (emitter) and center of circle is the correct bond length 2.55 Å. Right: Single-energy atomic image, crosses mark emitter and correct scatterer positions. Sources in all layers of slab.

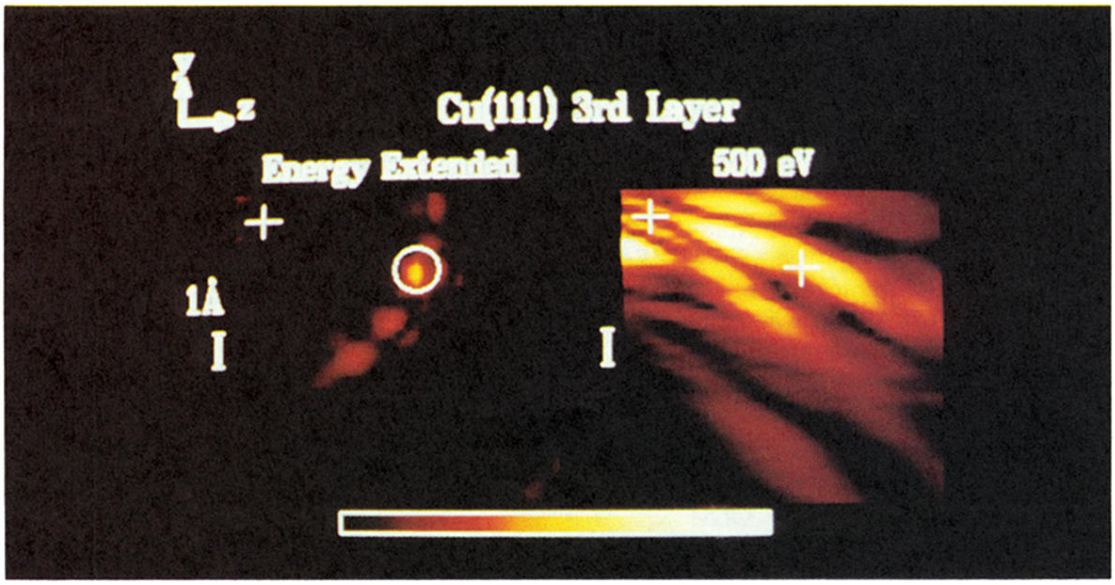


FIG. 8. Same as in Fig. 7 except along the 19.5° direction. Source atoms located in third layer only. The distance between emitter and scatterer is 4.42 Å.